JOURNAL OF BACTERIOLOGY, Dec. 1993, p. 7550–7560
0021-9193/93/237550-11$02.00/0

Vol. 175, No. 23

Characterization of the Cell Wall of the Sheathed Methanogen *Methanospirillum hungatei* GP1 as an S Layer

MAX FIRTEL,[1] GORDON SOUTHAM,[1] GEORGE HARAUZ,[2] AND TERRY J. BEVERIDGE[1]*

Department of Microbiology[1] and Department of Molecular Biology and Genetics,[2] College of Biological Sciences, University of Guelph, Guelph, Ontario, Canada N1G 2W1

Received 16 June 1993/Accepted 27 September 1993

The cell wall of *Methanospirillum hungatei* GP1 is a labile structure that has been difficult to isolate and characterize because the cells which it encases are contained within a sheath. Cell-sized fragments, 560 nm wide by several micrometers long, of cell wall were extracted by a novel method involving the gradual drying of the filaments in 2% (wt/vol) sodium dodecyl sulfate and 10% (wt/vol) sucrose in 50 mM *N*-2-hydroxyethylpiperazine-*N'*-2-ethanesulfonic acid (HEPES) buffer containing 10 mM EDTA. The surface was a hexagonal array ($a = b = 15.1$ nm) possessing a helical superstructure with a ca. 2.5° pitch angle. In shadowed relief, the smooth outer face was punctuated with deep pits, whereas the inner face was relatively featureless. Computer-based two-dimensional reconstructed views of the negatively stained layer demonstrated 4.0- and 2.0-nm-wide electron-dense regions on opposite sides of the layer likely corresponding to the openings of funnel-shaped channels. The face featuring the larger openings best corresponds to the outer face of the layer. The smaller opening was encircled by a stalk-like mass from which 2.2-nm-wide protrusions were resolved. The cell wall in situ was degraded at pH 9.6 at 56°C but was unaffected at pH 7.4 at the same temperature. The cell wall was composed of two nonglycosylated polypeptides (114 and 110 kDa). The cell wall resembled an archaeal S layer and may function in regulating the passage of small (<10-kDa) sheath precursor proteins (G. Southam and T. J. Beveridge, J. Bacteriol. 174:6460–6470, 1992).

The archaea are phylogenetically distinct from the eubacteria, and three basic phenotypes are recognized: methanogenic, halophilic, and sulfur-dependent thermophilic types (46). With few exceptions, the envelope of archaeal cells consists of a paracrystalline protein layer (S layer), one protein molecule thick, which is directly apposed to the plasma membrane (PM) (16; reviewed in references 15 and 23). Unlike more-rigid wall layers such as peptidoglycan, S layers are highly porous and non-cross-linked (16, 23) and have permeability properties similar to those of ultrafiltration membranes (30). Consequently, archaeal cells possessing an S layer as the sole component of the cell wall (CW) tend to stain gram negatively (15). S layers are often classified on the basis of their lattice symmetry (13); oblique (p2), tetragonal (p4), and hexagonal (p6) symmetries have been recognized. As a rule, archaeal S layers are hexagonally ordered (p6); exceptions include the tetragonal (p4) S layer of *Desulfurococcus mobilis* (45) and *Sulfolobus acidocaldarius*, which has recently been reclassified with the simpler p3 symmetry (20). The characteristic structural features of members of the orders *Thermoproteales* and *Sulfolobales* and of other archaeal S layers include layer-transversing channels and protrusions from the inner face that extend to the PM (1). Despite their prevalence and strategic location on the cell, a common underlying function for these protein layers has not yet been discovered (1, 4, 23).

Archaeal S layers are usually composed of homogeneous protein monomers that are held in a single layer by noncovalent intermolecular bonds (15, 23). However, glycosidic linkages have been identified in some archaeal S-layer monomers, particularly in extreme halophiles (19, 21), the proteins of which require additional polyanionic charges to counterbalance the effects of high salt on S-layer stability (15, 23). S-layer polypeptides are typically rich in nonpolar and acidic amino acid residues and are deficient in cysteine and methionine (16); however, a cysteine-rich region has been found in two thermophilic methanogen species (8).

The sheathed methanogen *Methanospirillum hungatei* (10) possesses an unusual external paracrystalline layer (i.e., the sheath) that differs from classical archaeal S layers for reasons including low porosity to solutes (6), few but strategic cross-linkages involving cysteine (35, 37), heteropolymer polypeptide composition (35), oblique (p2) lattice with exceptionally fine lattice packing (repeat of 2.8 by 5.6 nm) (41), assembly based on discrete hoop-like structures (37), and open-ended design (37). The cross-linkages produce an unusually stable layer that resists dissociation by conventional treatments (7, 28, 33, 37). A likely candidate for a more typical S layer is the CW (previously known as the inner wall [39]), which in thin sections is observed apposed to the tripartite PM bilayer and is involved in septation (3). However, direct observation of the CW in situ by negative stains or metal shadowing has not been achieved because of the overlying sheath, which is difficult to remove. The characterization of the CW layer is further complicated by its inherent instability once isolated from partially lysed filaments (38). As a consequence of these technical difficulties, the structure of the *M. hungatei* CW layer has not been satisfactorily resolved and its resemblance to archaeal S layers has yet to be confirmed.

The purpose of this study was to resolve the structural and chemical characteristics of the *M. hungatei* CW layer. A two-dimensional structure of the layer obtained from platinum-shadowed and negatively stained single-layer fragments is presented along with some preliminary observations of its chemical composition.

* Corresponding author. Electronic mail address: terry@Vm.Uoguelph.ca.

MATERIALS AND METHODS

Bacterial growth conditions. *M. hungatei* GP1 (27) (DSM 1101) was grown in 1-liter Wheaton flasks containing 100 ml of SA medium (26). The flasks were pressurized daily with a H_2-CO_2 (80:20) gas mixture.

S-layer preparation. Cells were harvested from culture by centrifugation at 15,000 × *g* for 10 min and washed once with deionized H_2O (dH_2O). A 200-mg (wet weight) sample of washed cells was suspended in 2.0 ml of the extraction buffer consisting of 2% (wt/vol) sodium dodecyl sulfate (SDS; Bio-Rad, Richmond, Calif.) and 10% (wt/vol) sucrose dissolved in 50 mM *N*-2-hydroxyethylpiperazine-*N'*-2-ethanesulfonic acid (HEPES) buffer (pH 6.8) with 10 mM EDTA. The suspension was placed in a watch glass and allowed to dry to a thick paste at room temperature in air. Evaporation was facilitated by gently flowing air from an in-laboratory air pressure line over the surface of the suspension. Enough dH_2O was added to the paste to reconstitute the original volume, and the resuspended cells were pooled with an additional half-volume of dH_2O used to collect the remaining residue in the watch glass. Unextruded filaments and aggregates were sedimented by low-speed centrifugation at 8,000 × *g* for 4 min. The cloudy supernatant containing the extracted material was centrifuged at 29,000 × *g* for 60 min, and the resulting pellet was resuspended in 20% (wt/vol) sucrose in 50 mM HEPES buffer containing 10 mM $NiCl_2$ as a potential structure stabilizer and 0.03% sodium azide as an antimicrobial agent. To improve the consistency of the negative stains, the extract was dialyzed against several changes of buffer for 24 h at room temperature to remove the SDS. The dialyzed extract was centrifuged at 29,000 × *g* for 60 min, the supernatant was removed, and the pellet containing the CW and contaminating particulates was kept at 4°C.

High heat (ca. 90°C) solubilized the CW as well as other cellular constituents and was unsuitable as an enrichment step for CW material. To determine the effect of milder heat on the solubilization of the CW, 10.0 mg (wet weight) of the pelleted material was suspended in 1.0 ml of phosphate buffer (pH 7.4) and heated in a heating block to 56°C for 30 min. The heat-insoluble and -soluble materials were separated by centrifugation at 29,000 × *g* for 60 min and analyzed for intact CW by transmission electron microscopy (TEM) (negative staining) and SDS-polyacrylamide gel electrophoresis (PAGE).

To determine the effect of sucrose alone on the CW, filaments were plasmolyzed and prepared for thin section as previously described (35).

Alkali treatment of whole filaments. Exponentially grown cells were harvested and washed in dH2O, and 100 mg (wet weight) of packed cells was suspended in 1.0 ml of phosphate buffer (pH 7.4) or 1.0 ml of carbonate-bicarbonate buffer (pH 9.6). The filaments were incubated at 56°C in a heating block for 30 min. After the treatment the filaments were prepared for embedding by washing twice with 50 mM HEPES buffer containing 10 mM $NiCl_2$ (pH 6.8) and fixing with glutaraldehyde as described below. An portion of the washed (unfixed) treated cells was reserved for protein analysis by SDS-PAGE.

TEM (i) Negative stain. The extracted material was diluted in 0.1% (wt/vol) sterile peptone in dH_2O and adsorbed on to carbon Formvar-coated copper grids (200 mesh) by floating the grids on a droplet of the sample placed on a sheet of Parafilm. After 2 min, the grids were removed and the excess suspension was withdrawn with filter paper, leaving a wet film. The specimens were floated on dH_2O to remove sucrose and buffer salts and transferred to a drop of 2% (wt/vol) aqueous ammonium molybdate (AM; pH 7.5) or 2% (wt/vol) aqueous uranyl acetate (UA; pH 4) for 5 to 15 s. The stained specimens were placed facedown on filter paper to dry and viewed the same day. The stains were filtered through a 0.22-μm-pore-size Millipore filter immediately prior to use.

(ii) Platinum shadowing. A Balzers high-vacuum freeze-etch unit (BA 360 M) equipped with evaporator guns and a quartz crystal monitor for estimating film thickness was used. The unit was operated by standard procedures and without cooling. The dialyzed extract was dried on a carbon Formvar-coated copper grid (200 mesh), rinsed two to three times with filtered dH_2O, and mounted on a custom-made Plexiglass sample holder prior to insertion into the unit. Fixed-angle shadowing at a deposition angle of 45° was used to deposit the platinum film, which was then backed with a carbon film. The film was deposited under a vacuum of 8×10^{-6} torr (ca. 11×10^{-4} Pa). The platinum film thickness was 1.4 nm.

(iii) Embedding for thin section. The cells were suspended in a fixative mixture containing 2% (vol/vol) glutaraldehyde (Marivac Ltd., Halifax, Nova Scotia, Canada) and 0.2% (vol/vol) formaldehyde in 50 mM HEPES buffer containing 10 mM $NiCl_2$ (pH 6.8) for 4 h and then washed in the same buffer without fixative. The cells were double fixed in 1% (vol/vol) osmium tetroxide in HEPES for 1 h and washed three times, the last time in dH_2O. The postfixed cells were enrobed in 2% (wt/vol) Noble agar and submerged in 2% (wt/vol) aqueous UA for 1 h to provide additional contrast. Dehydration occurred in a graded acetone series starting with 50% (vol/vol) acetone, followed by 75% (vol/vol), 95% (vol/vol), and three 100% acetone changes (made anhydrous by the use of a molecular sieve; Sigma Co., St. Louis, Mo.) for 15 min at each stage. Dehydrated samples were placed in acetone-Epon 812 (1:1) and allowed to infiltrate for 3 h in closed vials and overnight with the caps removed. The samples were transferred to fresh Epon 812 in flat embedding molds and cured at 60°C for 36 h. Silver sections were cut with an Ultracut E Reichert-Jung ultramicrotome, collected on carbon Formvar-coated grids, and stained with 2% (wt/vol) UA for 15 min and 2% (wt/vol) lead citrate for 10 min.

The specimens were viewed with a Philips 300 electron microscope operating at 60 kV under standard conditions with a liquid-nitrogen cold trap in place. The primary magnification for photographing negatively stained and thin-sectioned specimens was ×22,800, and that for Pt-shadowed specimens was ×14,148.

Image processing. Electron micrographs of negatively stained CWs were assessed for optimal focus and astigmatism by optical diffraction, and two micrographs showing apposing surface views were selected for image processing. Video images were obtained with a Hitachi KP-113 solid-state television camera mounted on a dissecting microscope equipped with 16× and 64× objectives (Wild Leitz M3B). Digital processing was performed with IMAGIC software (12) supported by MS-DOS on a personal computer. Lattice symmetry and spacing were determined from computer-generated diffraction patterns by using digitized areas corresponding to several hundred unit cells. Correlation averaging was used for high-resolution image reconstruction of individual unit cells since this technique is insensitive to long-range lattice imperfections (31). For correlation averaging, ×16- or ×64-magnified views of the micrographs, depending on the ease with which the unit cells could be identified, were used. The micrographs were digitized in small patches, and the most easily identifiable unit cells were extracted and collected in a master file. Over 100 unit cells, each with its surrounding perimeter, were extracted. The molecular positioning of the unit cells was determined relative to the reference motif, and the extracted unit cell images displaying the best correlative values were superim-

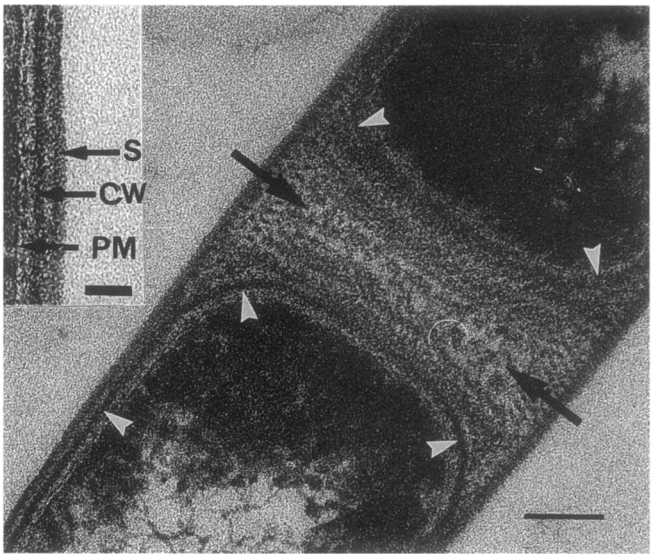

FIG. 1. Longitudinal thin section of an *M. hungatei* GP1 filament showing the typical end-to-end alignment of neighboring cells. The cells are bounded by the CW (white arrowheads) and are separated from each other by a spacer region (dark arrows) bounded by spacer plugs. Bar = 100 nm. The inset is a detail of the cell envelope. S, sheath. Bar = 40 nm.

posed and averaged. Fourier-filtered reconstructed images were used for the reference motif. The results are displayed in a grey scale in which brightness maxima and minima correspond to areas in the original micrograph of maximum stain exclusion and pooling, respectively.

SDS-PAGE. Electrophoresis was performed by the method of Laemmli (18) in a minigel system (Bio-Rad); 18% (wt/vol) acrylamide was used for the separating gel. Whole filaments and other particulate extracts were prepared for electrophoresis by boiling 2 μl of sample in 20 μl of lysis buffer containing 5% (vol/vol) β-mercaptoethanol and 2% (vol/vol) SDS. All other samples were prepared by adjusting the protein concentration to 0.5 to 1.0 mg/ml (measured by the bicinchoninic acid method; Pierce, Rockford, Ill.) in phosphate buffer (pH 7.4). Mixtures containing equal volumes of sample and lysis buffer containing β-mercaptoethanol and SDS were boiled for 5 min prior to loading into wells. Electrophoresis was performed at a constant 110 V.

Gels were stained for protein with 0.5% (wt/vol) Coomassie brilliant blue (Sigma) in 40% (vol/vol) methanol–10% (vol/vol) acetic acid for 1 h at room temperature or with ammoniacal silver nitrate. Low- and high-molecular-weight markers (Sigma) were loaded with each gel. Gels were stained for glycoprotein by the periodic acid-Schiff method described by Fairbanks et al. (9). Bovine A-1 glycoprotein (Sigma) was used as a positive control.

RESULTS

Envelope structure of *M. hungatei* GP1. The complex envelope profile typical of *M. hungatei* (3) was observed, and an example is shown in longitudinal section in Fig. 1. Electron-dense layers corresponding to the sheath (ca. 9.0 nm thick) and CW (ca. 10.0 nm thick), which encloses the cell, were separated by an electron-translucent zone (ca. 8.0 nm thick). The periodicity of the CW layer was discerned only in cross-sectioned views. The PM was tripartite (i.e., an electron-translucent zone sandwiched between electron-dense layers), ca. 6.5 nm thick, and completely overlaid by the CW layer. Unlike that in other methanogens such as *Methanococcus voltae* (17), the CW was separated from the PM by a zone of weakly staining material (ca. 8.0 nm thick). The electron-dense layers of the multilayered plug, which were found associated with the polar regions of the cell, spanned the inner circumference of the sheath and displayed periodic ordering. The adhesive material that joins the plug structure to the CW (37, 38) was observed.

General description of the cell extract prepared as whole mounts. In a preliminary study, harvested and washed *M. hungatei* filaments were suspended in HEPES buffer (pH 6.8) with or without added 2% (wt/vol) SDS detergent and allowed to dry directly on TEM support grids. The filaments dried in HEPES alone remained intact; the collapsed sheath tubule was filled with cellular material which condensed into long, thin rods (not shown). Filaments dried in the presence of SDS were partially lysed, and cellular material was observed to extrude through the sheath at intervals along the length of the filament (Fig. 2). Occasionally, an external layer presumed to be the CW detached from the extruded portion of the cell cytoplasm. While a hexagonal array could be discerned in the detached layers, the staining was generally of poor quality due to the interference of trace amounts of detergent in the preparation on the metal stain. For this reason, platinum-shadowed preparations proved best for visualizing the CW.

To improve the collection and staining of the CW layer, filaments were lysed in 2.0-ml quantities in a watch glass by the method described. Typically 20 to 30 min was required for drying. Low-speed centrifugation (8,000 × *g*) of the rehydrated mixture separated large aggregates of intact filaments from extracted material which consisted of CW, lysed fragments, and soluble and insoluble cytoplasmic material. The particulate material was separated from the soluble material by high-speed centrifugation (29,000 × *g*). From 100 mg (wet weight) of whole filaments about 9 to 10 mg (wet weight) of crude particulate material was obtained.

The particulate extract was dialyzed to remove excess SDS and prepared for negative staining or platinum shadowing. The periodicity of the CW surface was evident by either method of preparation. Cell-sized CW fragments, 565 nm wide and of variable length (1,000 to 3,000 nm), were commonly found, and a typical example is shown in relief in Fig. 3. These CW fragments were distinguished from contaminating sheaths by their hexagonal array and from plug layers by their rectangular shape and greater size. Moiré patterns indicative of multilayered sheets were evident in negative stains of well-preserved CW fragments (not shown). Examination of these fragments in relief indicated that they were the cylindrical portion of CW that had collapsed onto themselves to form flattened tubes. Completely intact cell envelopes were not observed, and the cell poles were found only entrapped within sheath contaminants. Filaments exposed to a hypertonic solution of sucrose in the absence of detergent were observed to develop breaks in the CW near the cell poles (Fig. 4). Remnants of cytoplasmic material or PM were observed attached to the CW as thin fibrils or small (50-nm or less) clumps or sheets. Long-range structure was recognized in well-preserved CW fragments; one symmetry axis was measured at ca. 2.5° from the normal to the long axis of the rod-shaped cell, indicating a helical superstructure (the pitch angle was based on measurements of a right triangle composed of intersecting longitudinal [base], symmetry [hypotenuse], and cross [perpendicular] axes).

A suspension of the dialyzed CW extract made in 50 mM HEPES-buffered sucrose (20% [wt/vol]) containing millimolar amounts of Ni was monitored daily during storage at 4°C by

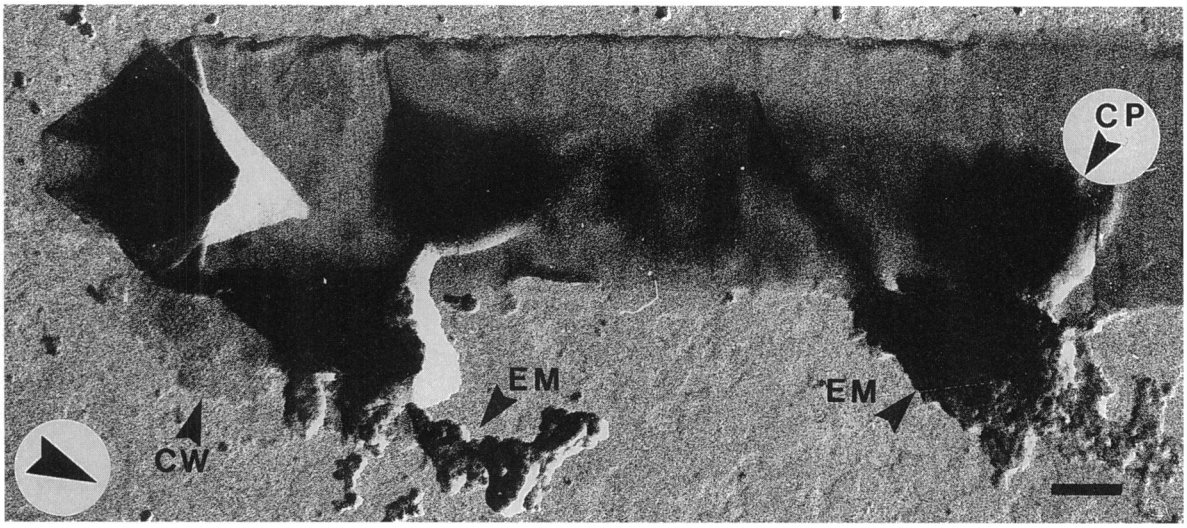

FIG. 2. Platinum-carbon-shadowed *M. hungatei* filament dried on the electron microscopy support grid in the presence of SDS. The filament terminus is shown at the left. EM, extruded cell material; CP, cell pole (confined within sheath). The large arrowhead indicates the shadowing direction. Bar = 100 nm.

TEM. Initially, the periodicity of the CW was evident in the majority of cell-sized fragments. After 3 to 4 days, cell-sized fragments possessing a hexagonal array were difficult to find and by 7 days could not be observed in any of the fragments. The rapid dissociation of the isolated CW was achieved by heating the dialyzed extract to 56°C in phosphate buffer.

Asymmetry of the faces of the CW. On occasion, single-layer sheets of CW were found where the cylinder had unravelled (Fig. 3). Two distinct surface morphologies were observed in these single-layer sheets in negative stains with either 2% (wt/vol) UA (Fig. 5 and 6) or 2% (wt/vol) AM (not shown). AM staining produced patterns similar to those produced by UA, but AM staining was of lower contrast. One face was characterized by electron-dense circular depressions ca. 8 nm wide (Fig. 5). The opposite face varied in appearance depending on the type and length of exposure of the stain; the most complex patterns were revealed with a 15-s exposure to UA stain (Fig. 6). This face was more structured than the opposite face and consisted of electron-dense circular depressions ca. 2.0 to 3.0 nm wide surrounded by electron-dense oblong grooves (9.0 nm long by 3.0 nm wide) that roughly formed a hexagon. The computer-generated transforms obtained for

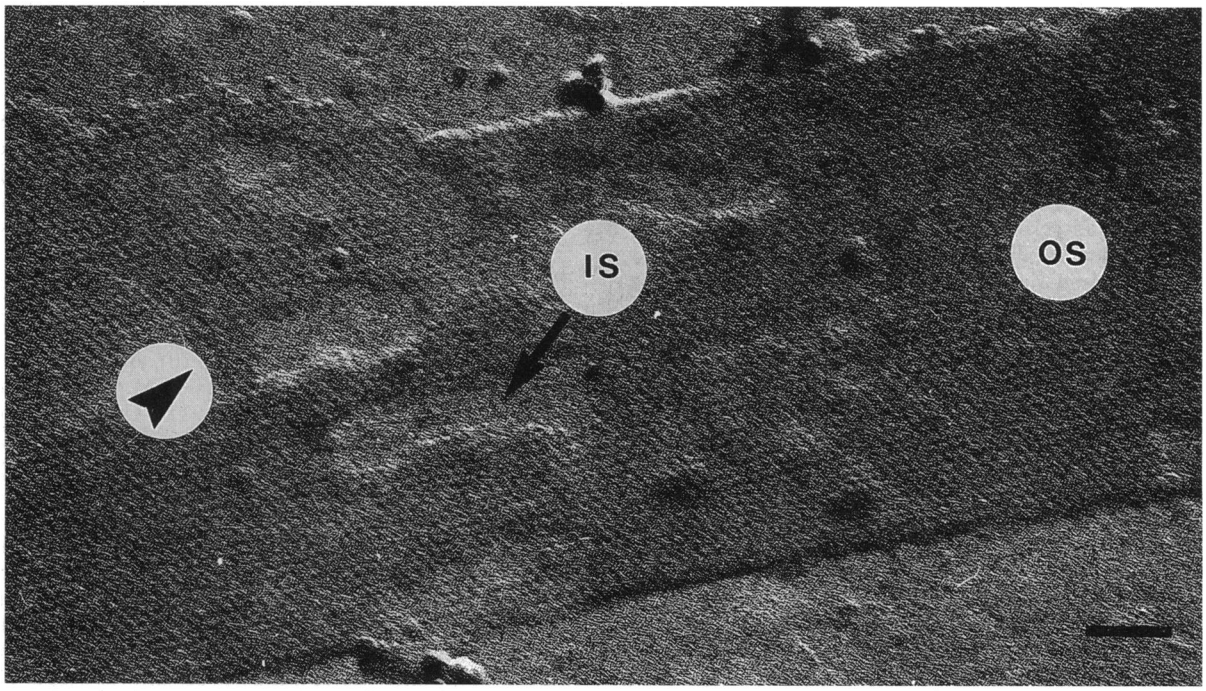

FIG. 3. Platinum-carbon-shadowed cylindrical fragment of the CW with the outer surface (OS) and a small region of the inner surface (IS) exposed. The arrowhead indicates the shadowing direction. Bar = 100 nm.

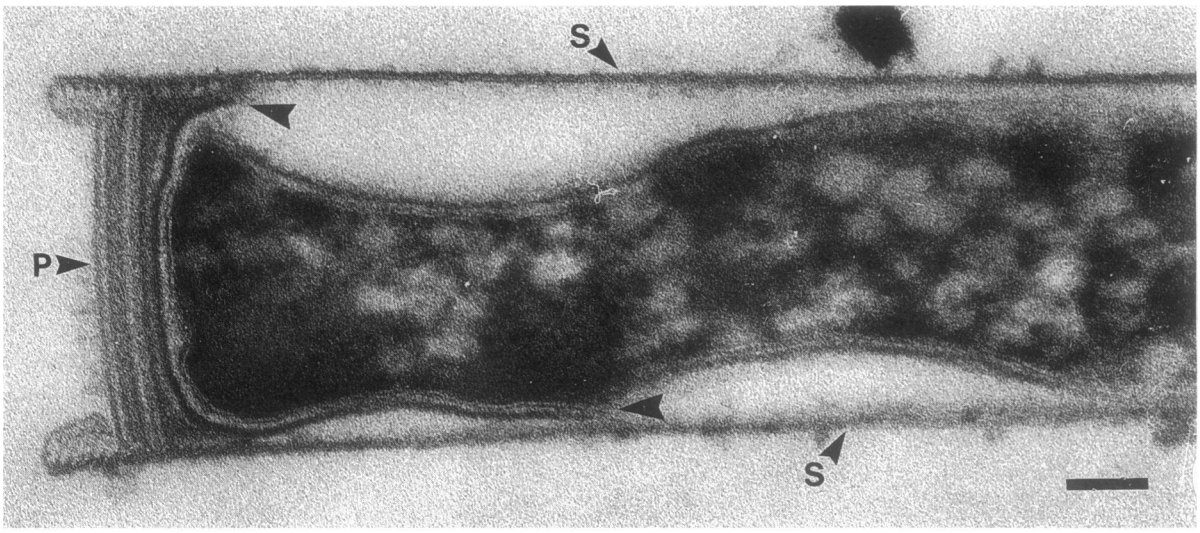

FIG. 4. Thin section of plasmolyzed filament kept in 30% (wt/vol) sucrose. The polar CW breaks (large arrowheads) but remains attached to the plug (P). S, sheath. Bar = 100 nm.

each surface demonstrated a single set of strong reflections along sixfold axes spaced 15.1 nm apart. The transforms were indicative of single layers and provided evidence for facial asymmetry in the CW layer. Reflections were found in both faces extending to the fourth order, corresponding to a resolution of ca. 3.0 nm. Strong first- and second-order reflections were found in the more structured face, as expected for its complex morphology (Fig. 6). The structure in the smoother face was largely contained within the first-order reflections (Fig. 5).

These two surfaces could not be distinguished as the outer and inner faces in negative stains, and shadowed relief views were examined in an attempt to identify them. The comparison of relief and negatively stained views could be achieved only on the basis of the most prominent structural details since the grain of the platinum film obscured fine detail. In relief, the outer surface consisted of circular pits distributed as a hexagonal array spaced ca. 15 nm (Fig. 3). The topology of the outer face was consistent with a smooth surface punctuated by large openings and best corresponded to the surface shown in Fig. 5. The inner face was relatively featureless, and no obvious details could be discerned.

High-resolution reconstruction of both faces. Since lattice disorder in exposed single layers was apparent by eye, high-resolution reconstructions were performed by the correlation averaging method. The reconstructed views are given with superimposed contours indicating differences in grey intensity in Fig. 7 and 8. As expected, correlation averaging led to an improvement in the resolution of the structure compared with that by the Fourier filtering; the calculated resolutions of the outer smooth and inner structured faces were 2.5 and 2.9 nm, respectively. The electron-dense circular depressions were situated at the center of each unit cell, which suggested that they were the opposite openings of a continuous channel through the depth of the layer. The openings were measured across the darkest region (brightness minima) to yield a minimum diameter for the channel exits. The minimum diameters of the openings in the smooth (Fig. 7) and structured (Fig. 8) faces were 4.0 and 2.0 nm, respectively, suggesting a funnel-shaped channel running from outside to inside through the CW. Given the thickness of the CW from thin-section data (i.e., 10 nm), the total volume occupied by the pore was calculated to be ca. 290 nm^3 by using the geometrical formula for determining the volume of a truncated cone. The mass (i.e., the stain-excluding regions) in the face possessing the 4.0-nm opening interconnected with neighboring unit cells and was slightly contoured. On the opposite face, the mass surrounding the 2.0-nm opening was highly contoured and isolated from neighboring unit cells by oblong depressions measuring 8.7 by 3.0 nm. Fine structural detail in the oblong depressions corresponded to the contours previously observed in the interconnected mass of the opposite face. The isolated mass was 12.0 nm wide and had a stalk-like appearance. Oval protrusions (2.2 by 1.9 nm) arranged along sixfold axes were resolved at the base of the mass. Handedness was not observed in any of the resolved features. A conceptual cross-sectional view of the CW layer and its associated layers in the cell envelope is given in Fig. 9.

Analysis of CW proteins by SDS-PAGE. With whole, untreated *M. hungatei* filaments as the sample, 11 major polypeptide bands and numerous lesser bands were observed in 18% (wt/vol) acrylamide gels stained with Coomassie blue dye. The two most prominent polypeptides have molecular masses of 114 and 110 kDa. Of all the major bands, only the 114-, 110-, 74-, and, to a lesser extent, 45-kDa bands were found in the insoluble extract (Fig. 10). Heating the extracted fraction in pH-neutral phosphate buffer for 30 min at 56°C solubilized both the 114- and 110-kDa polypeptide bands (Fig. 10), and this was concomitant with a loss of CW observable by TEM. Although both the 114- and 110-kDa bands were stained by Coomassie blue dye, they could not be stained by the silver staining method used for protein detection. Further, the 114- and 110-kDa polypeptide bands were periodate-Schiff negative in gels. These results indicate that the 114- and 110-kDa polypeptides have similar amino acid compositions and periodate-sensitive carbohydrate moieties may not account for the difference in their masses.

In contrast to the isolated CW, heating intact untreated filaments for 30 min at 56°C failed to solubilize the 114- and 110-kDa polypeptides (Fig. 11), demonstrating the stability of the CW in situ. Solubilization of the 114-kDa–110-kDa polypeptide couplet could be achieved by treating whole filaments for 30 min at 56°C at pH 9.6 in 50 mM bicarbonate

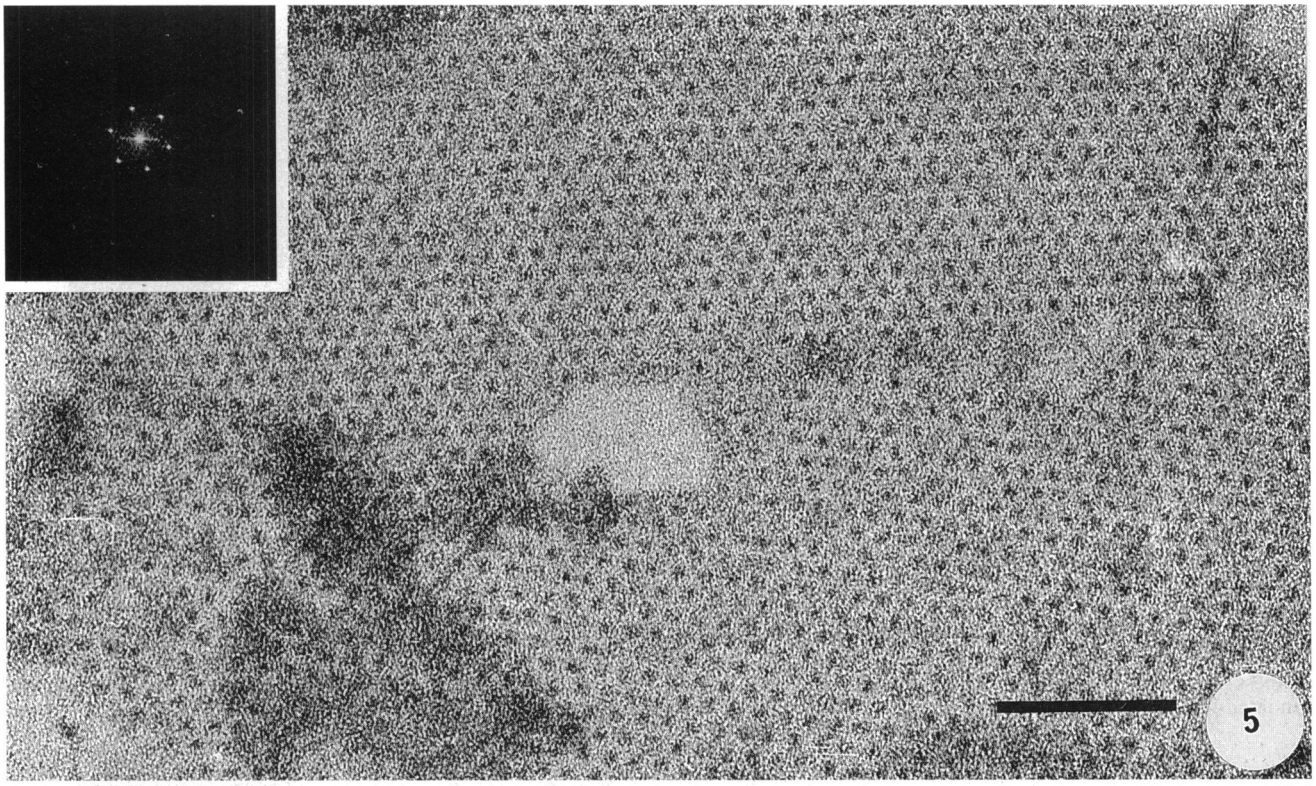

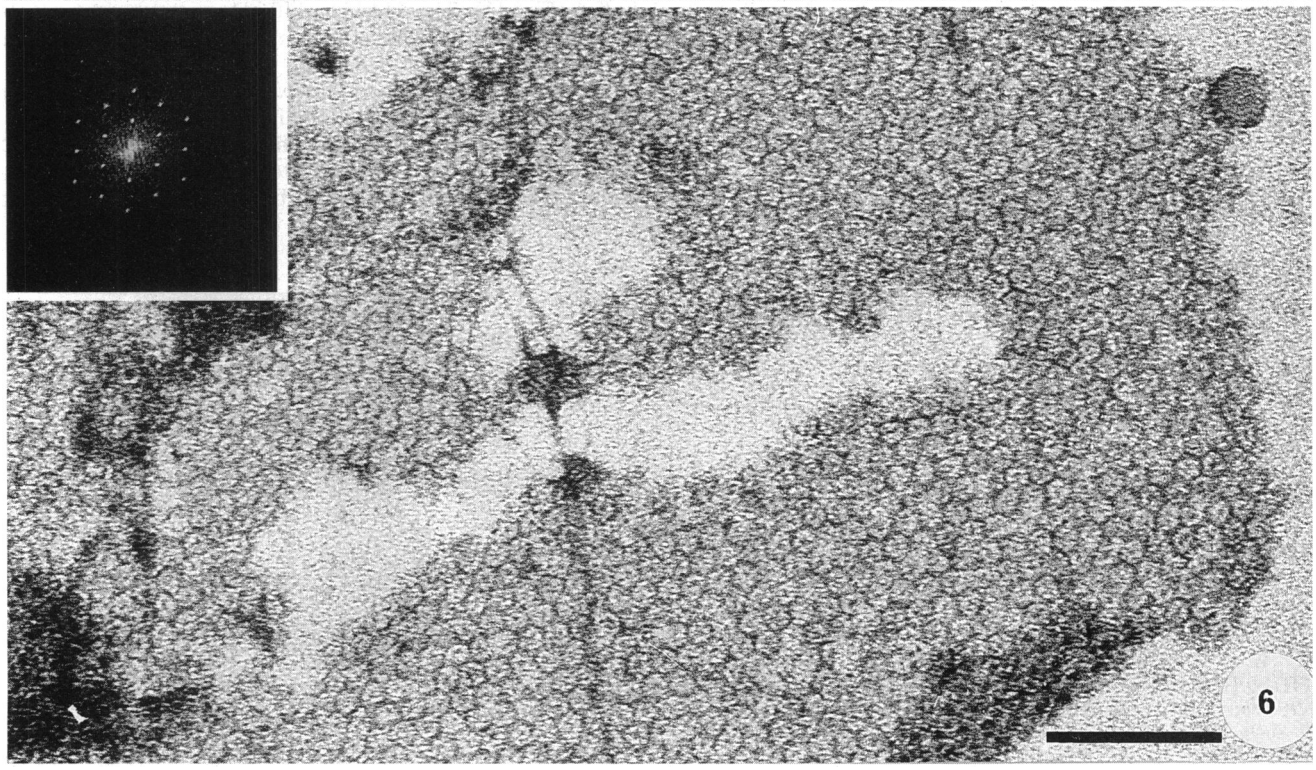

FIG. 5. Negatively stained CW monolayer with the smooth face exposed. Bar = 100 nm. The inset shows the computer-generated transform derived from a 65,000-nm^2 area of the layer.

FIG. 6. Negatively stained CW monolayer with the structured face exposed. Bar = 100 nm. The inset shows the computer-generated transform derived from a 65,000-nm^2 area of the layer.

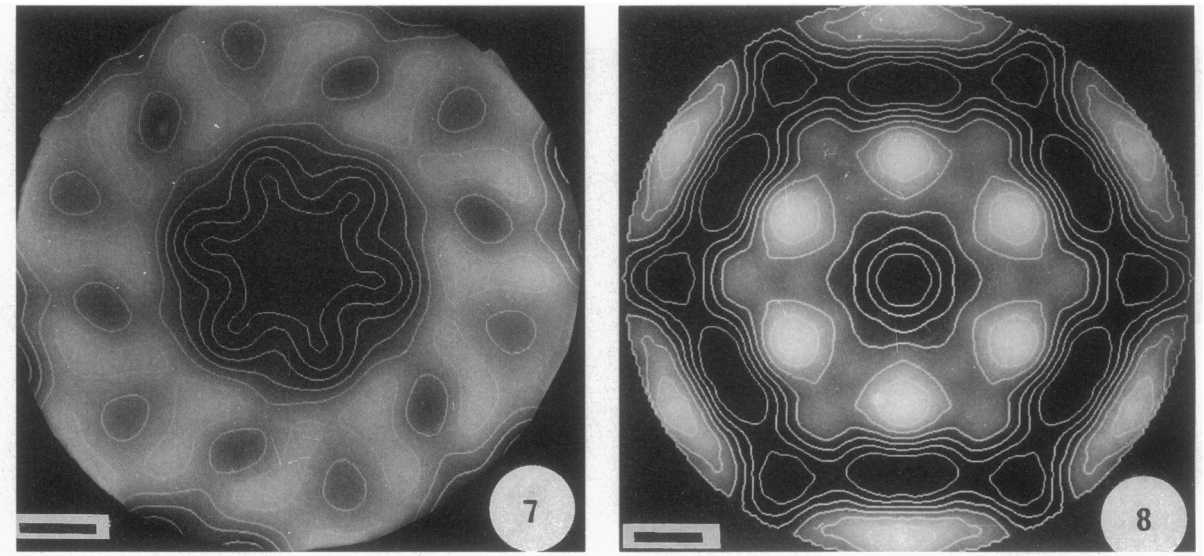

FIG. 7. Computer reconstruction of the unit cell observed in the outer smooth face (Fig. 5). Over 350 unit cells were extracted from digitized ×16-magnified views of the original micrograph. Sixfold rotational symmetry was imposed. Contrast due to stain pooling is indicated by brightness levels; minimal levels correspond to areas of greatest pooling. The contour lines indicate levels of grey intensity above and below the mean intensity. Bar = 2.0 nm.

FIG. 8. Computer-reconstructed view of the unit cell observed in the inner structured face (Fig. 6). Over 100 unit cells were extracted from digitized ×64-magnified views of the original micrograph. Sixfold rotational symmetry is imposed. Contrast due to stain pooling is indicated by brightness levels; minimal levels correspond to areas of greatest pooling. The contour lines indicate levels of grey intensity above and below the mean intensity. Bar = 2.0 nm.

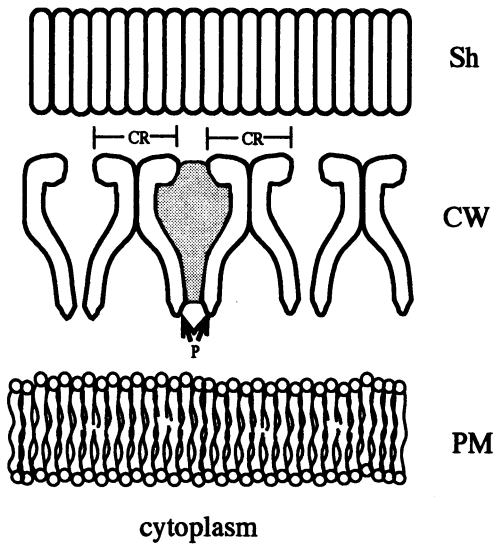

FIG. 9. Conceptual cross-sectional view of the *M. hungatei* CW layer based on two-dimensional reconstructions of negatively stained CW surfaces. Individual monomers are shown as comma-shaped structures that join to neighboring monomers at the outer surface of the layer (connective regions; CR), forming a canopy, and curve towards the center of the unit cell to form the stalk. Situated at the base of the stalk are the 2.2-nm projections (P) which may interact with the PM (shown as lipid bilayer). The funnel-shaped stain-filled channel of the unit cell is shown (dark shading). Schematic 2.8-nm repeat units of the sheath layer (Sh; ovals) are also shown. For clarity, only two monomeric polypeptides per unit cell are depicted. Not to scale.

buffer (Fig. 11). The 114-kDa–110-kDa couplet was not observed in the alkali-soluble fraction which was found to contain polypeptides of lower molecular mass, the most prominent being ca. 25 kDa, indicating that extensive protein degradation had occurred under alkaline conditions.

Envelope profile of *M. hungatei* filaments incubated at 56°C. Whole filaments were incubated to 56°C for 30 min in phosphate (pH 7.4) or carbonate-bicarbonate (pH 9.6) buffers and

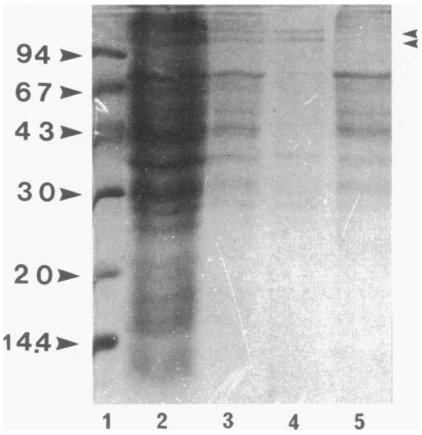

FIG. 10. SDS-polyacrylamide gel stained with Coomassie blue dye to demonstrate the position of the prominent protein bands during the extraction procedure. Lanes: 1, molecular weight markers; 2, low-speed pellet; 3, high-speed pellet; 4, heat-solubilized fraction of high-speed pellet; 5, heat-insoluble fraction of high-speed pellet. The CW-associated polypeptides (i.e., the 114- and 110-kDa polypeptides) are indicated by small arrowheads. The marker positions (in kilodaltons) are indicated by large arrowheads.

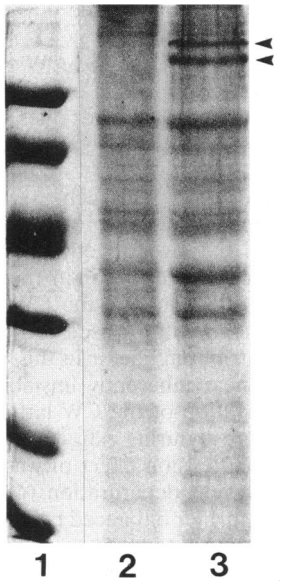

FIG. 11. SDS-polyacrylamide gel stained with Coomassie blue dye to demonstrate the positions of the prominent protein bands derived from whole filaments heated to 56°C to liberate the cell wall polypeptides. Lanes: 1, molecular weight standards; 2, insoluble fraction of filaments heated in bicarbonate-carbonate buffer (pH 9.6); 3, insoluble fraction of filaments heated in Sorensen's phosphate buffer (pH 7.4). Arrowheads indicate the positions of the 114- and 110-kDa bands.

prepared for thin sectioning. At a pH of 7.4, the envelope structure remained unaltered by incubation at 56°C (Fig. 12) compared with that of untreated controls (Fig. 1). The periodic nature of the sheath or CW was rarely observed.

The cell envelope was degraded by incubating the filaments at a pH of 9.6 (Fig. 13). An electron-translucent space (ca. 30 nm wide) existed between remnants of the PM and the inner face of the sheath (recognized by its 2.8-nm circumferential repeat). From careful examination of this zone it was concluded that the CW material was dispersed and no longer in the form of a layer. The cytoplasm was largely missing, although areas of congealed cytoplasm could be found associated with intact stretches of PM. The solubilization of the CW layer by alkali was associated with the disappearance of the 110-kDa–114-kDa couplet (Fig. 11).

DISCUSSION

In this study, a novel slow dehydration method was used to isolate cell-sized CW fragments from *M. hungatei* filaments. Two-dimensional structural and chemical analyses of the isolated structure demonstrated a close resemblance of the *M. hungatei* CW to typical archaeal S layers (1, 13, 23). The CW was a hexagonal array with a lattice spacing and protein mass (repeat spacing [$a = b = 15.1$ nm]; molecular mass = 110 or 114 kDa) that were within the ranges reported for S layers from other methanogens, i.e., lattice spacings ranging from 9.8 to 19.2 nm and the monomeric masses ranging from 60 to 156 kDa (see Table 1 in reference 23). The cylindrical portion of the CW was found to be free of obvious lattice defects and possessed a helical superstructure of low pitch angle (ca. 2.5°). The CW in situ is sandwiched between heterologous envelope layers, and the effect may be reflected in asymmetrical faces of the CW layer. The porosity of the layer is likely regulated by funnel-shaped channels measuring 2.0 nm at their narrowest which are situated in the center of each unit cell. The CW is composed of nonglycosylated polypeptides that are a major protein component of the whole cell. Once separated from the sheath, the CW polypeptides were conveniently solubilized by

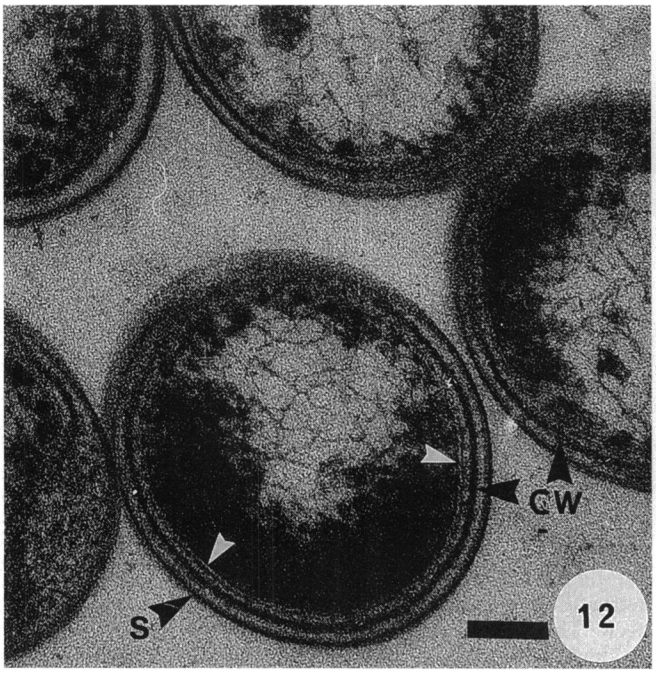

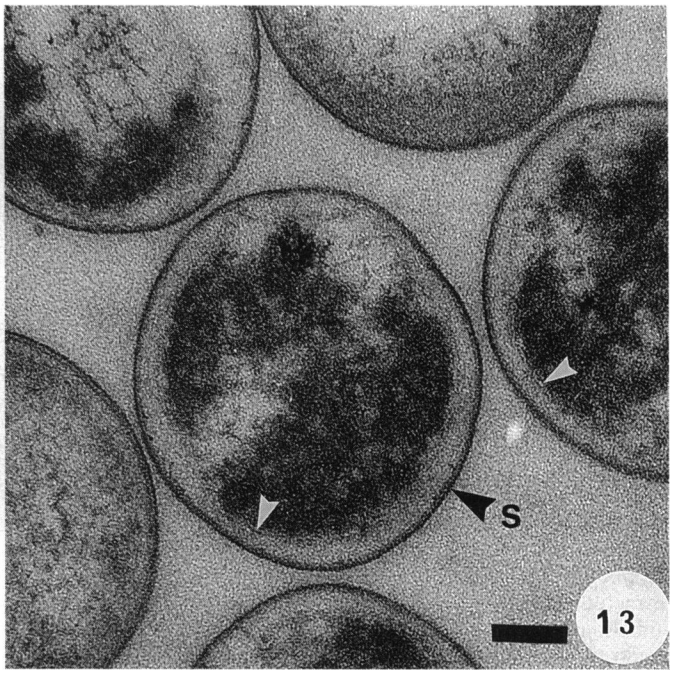

FIG. 12. Thin cross section of whole filaments heated to 56°C for 30 min in phosphate buffer (pH 7.4). S, sheath. White arrowheads indicate the PM. Bar = 100 nm.

FIG. 13. Thin cross section of whole filaments heated to 56°C for 30 min in bicarbonate-carbonate buffer (pH 9.6). The CW could not be observed. S, sheath. White arrowheads indicate the PM. Bar = 100 nm.

heating the extract to 56°C in pH-neutral phosphate buffer, indicating that the CW layer is probably stabilized by noncovalent bonds.

In *M. hungatei*, the cells are separated from the surrounding environment by the sheath and from their cellular neighbors by spacer plugs. These structures combine to protect the cell from osmotic stress and to act as a sieving barrier (6, 38). Since the cell is totally enclosed, the main function of its CW may be to regulate the passage of large solutes such as sheath precursor polypeptides (molecular mass = 10 to 40 kDa) (33) and phenol-soluble polypeptides (molecular mass = 62 to 66 kDa (35) to their incorporation sites. Assuming a continuous pore through the CW, the transversing proteins must be smaller than 2.0 nm in their smallest dimension to pass through the layer. Openings of this size would exclude proteins as small as cytochrome *c* (molecular mass = 12.4 kDa; 3.7 by 2.5 by 2.5 nm [42]) in their native conformation. This suggests that only unfolded forms of the sheath precursor and phenol-soluble polypeptides could be accommodated. The 10-nm-wide polar flagella found in this organism, as well as other methanogens, is an obvious exception to the normal exclusion limits imposed by the CW on large molecules. Flagellar extension through the CW may require specific accommodation sites which may disturb the lattice order of the layer. Lattice defects act as incorporation sites for new S-layer material and so are compatible with S-layer function (23). However, we have not been able to isolate suitable polar fragments for structural analysis since the polar regions break from the cylindrical regions and remain in the sheath through their firm attachment to the plug.

The scheme shown in Fig. 9 uses the archaeal S-layer design proposed by Baumeister et al. (1). In this model, neighboring unit cells are interconnected at the outer surface of the layer to form a canopy which is supported by stalks that extend from the inner surface to the underlying membrane. The basic design of the model was readily recognized in the reconstructed views of the *M. hungatei* CW layer. The smooth face, which was highly interconnected and punctuated with large openings, may correspond to the outer-facing canopy. The pitted outer surface of the CW layer shown in relief is consistent with this interpretation. The highly structured face consisted of rectangular trenches that were not continuous throughout the layer and that enscribed a stalk-like mass ca. 12.0 nm in diameter from which 2.2-nm-wide protrusions were detected. This enscribed mass may correspond to the canopy-supporting stalk. However, unlike the prominent stalks of the inner face of the rigid S layer from *Thermoproteus tenax* (1, 22), the stalks of the *M. hungatei* CW are not observed in either thin-section or shadowed-relief views, indicating a relatively truncated structure. Intriguingly, the 2.2-nm-wide protrusions situated at the base of the stalk may be domains that contact the PM or interact with linker material that spans the region between the PM and CW layers. There is a discrepancy between this interpretation of the 2.2-nm protrusions and the thin-section evidence, which fails to demonstrate a direct association between these envelope layers (3, 38). This envelope profile, however, is different from the envelope profile observed in other methanogens (2, 17), including *Methanosaeta* (*Methanothrix*) *concilii* (5), suggesting that the PM may have retracted from the CW during processing for conventional embedding. To explore the possibility of direct contact between the PM and CW layers of *M. hungatei* and account for the 2.2-nm protrusions, we are currently attempting to examine thin sections of cryopreserved filaments. A comparative study of conventional and cryogenic methods of embedding cells indicates the superiority of the latter method for accurately preserving cell ultrastructure in a wide range of bacterial types (11).

We have found that the extracted CW gradually becomes difficult to observe by TEM because of the increasing disorder of the array during storage. The layer does not dissociate into monomeric subunits on storage, suggesting that the CW monomers contain at least two domains: one domain which easily solvated in a polar environment such as water and another domain, likely hydrophobic, which provides the intermolecular links needed to hold the layer together. The easily solvated domain likely produces the disorder in the lattice which has caused the difficulty in identifying the CW in earlier studies (38, 40). The alkaline conditions used to isolate spheroplasts may have been a contributing factor in this difficulty since the CW polypeptides appear inherently unstable at high pH. In this study, the preservation of the CW lattice may have been due to the role of sucrose during extraction. Sucrose is known to increase the surface tension effect of water at the protein-water interface to prevent denaturation (43). The stabilizing effect may have been further enhanced by encasing of the layer in a sucrose shell during drying. Sucrose was insufficient for long-term stabilization of the isolated CW, and other factors need to be considered. The role of Ni as an envelope stabilizer is suggested from the finding of high levels of this cation in the *M. hungatei* PM (40). However, isolated CW did not give a strong Ni signal by energy-dispersive X-ray spectroscopy (not shown), and Ni did not appreciably prolong the longevity of the layer during storage. These observations indicate that Ni may not directly act to stabilize the CW layer, and its role in the envelope is unclear.

In the dehydration method used in this study, the force required to extrude the cells may have been caused by the collapse of the flexible sheath during drying (36). The force is insufficient to break the sheath layer unless breaks occur as a result of the detergent or sucrose present in the extraction buffer. These breaks in the sheath may occur through longitudinal lattice faults in the sheath (34) which become weakened during dehydration in sucrose (32a). The spacer plugs may support the collapsing sheath during drying and prevent the extrusion of the entire cell contents. Partial filament lysis was also observed in the structurally related *M. concilii* GP6 (5) by this method (unpublished observation), indicating its potential value in extracting the CW from these organisms. This manner of filament lysis differs from dithiothreitol-induced lysis, which depends on osmotic swelling of the cell to break through sheath destabilized by the thiol reducing agent (38).

Few eubacterial species (14, 25, 44) and only one archaeal species, namely, *Pyrobaculum organotrophum* H10 (29), have been previously shown to possess multilayered protein cellular envelopes. The companion layers in these organisms have identical crystal symmetries, although the spacing and protein mass distribution may vary. The importance of an assembled inner layer for assembly of the outer layer has been proposed for *Lampropedia hyalina* (25) and *Aquaspirillum serpens* MW5 (14). With the results of our study, *M. hungatei* may now be included in this rare group of organisms; however, it is now apparent that there is very little similarity in the structure and assembly of the companion array layers (i.e., sheath and plugs) in this organism. The sheath is an open-ended cylindrical structure, while the CW completely surrounds each rod-shaped cell. The sheath elongates in a combined process of hoop widening followed by circumferential splitting into two smaller hoops (35), whereas the extension of the CW probably occurs along helical axes in the manner proposed for *T. tenax*, i.e., by incorporation of new material at discrete sites in the polar region of the cell (22). While the sheath and CW appear to be

assembled by different routes, their regulation must be highly coordinated.

Two major polypeptide bands (molecular masses = 114 and 110 kDa) were found to be closely associated with the appearance of CW layer. The disintegration of the CW resulted in either the degradation or solubilization of the 114-kDa–110-kDa couplet. These polypeptides are not a major component of purified PM (40). Double S-layer monomer bands are not unusual and have been observed in a variety of organisms, including *Methanococcus jannaschii* (24) and the cyanobacterium *Synechococcus* strain GL (32). Superficially, the CW polypeptides resemble typical S-layer monomers since both bands fail to oxidize with periodate or to stain by the silver diamine stain method, indicating their deficiency in periodate-sensitive carbohydrates and free amine- and sulfur-containing amino acids. The 114-kDa–110-kDa polypeptide couplet was degraded by heating intact filaments in alkaline buffer. The degradation of the couplet also occurred with a preparation of cells sheared in a French press (not shown). The cause of the degradation is under investigation, and the role of alkali-activated proteolytic enzyme is being considered.

ACKNOWLEDGMENTS

We thank G. D. Sprott for his insights and advice and G. Patel for his helpful suggestions for growing the cells. We also thank B. Harris for his assistance in preparing platinum-shadowed specimens.

This work was funded by a Medical Research Council of Canada operating grant to T.J.B. The electron microscopy was performed in the NSERC Guelph Regional STEM Facility, which is partially maintained by an NSERC infrastructure grant to T.J.B.

REFERENCES

1. **Baumeister, W., I. Wildhaber, and B. M. Phipps.** 1989. Principals of organization in eubacterial and archaebacterial surface proteins. Can. J. Microbiol. **35:**215–227.
2. **Beveridge, T. J., C. G. Choquet, G. B. Patel, and G. D. Sprott.** 1993. Freeze-fracture planes of methanogen membranes correlate with the content of tetraether lipids. J. Bacteriol. **175:**1191–1197.
3. **Beveridge, T. J., B. J. Harris, and G. D. Sprott.** 1987. Septation and filament splitting in *Methanospirillum hungatei*. Can. J. Microbiol. **33:**725–732.
4. **Beveridge, T. J., S. F. Koval, U. B. Sleytr, H. König, and T. J. Trust.** 1993. Summary statements, p. 323–327. *In* T. J. Beveridge and S. F. Koval (ed.), Advances in bacterial paracrystalline surface arrays. Plenum Publishing Corp., New York.
5. **Beveridge, T. J., G. B. Patel, B. J. Harris, and G. D. Sprott.** 1986. The ultrastructure of *Methanothrix concilii*, a mesophilic aceticlastic methanogen. Can. J. Microbiol. **32:**703–710.
6. **Beveridge, T. J., G. D. Sprott, and P. Whippey.** 1991. Ultrastructure, inferred porosity, and Gram-staining character of *Methanospirillum hungatei* filament termini describe a unique cell permeability for this archaebacterium. J. Bacteriol. **173:**130–140.
7. **Beveridge, T. J., M. Stewart, R. J. Doyle, and G. D. Sprott.** 1985. Unusual stability of the *Methanospirillum hungatei* sheath. J. Bacteriol. **162:**728–737.
8. **Bröckl, G., M. Behr, S. Fabry, R. Hensel, H. Kaudewitz, E. Brendl, and H. König.** 1991. Analysis and nucleotide sequence of the genes encoding the surface-layer glycoproteins of the hyperthermophilic methanogens *Methanothermus fervidus* and *Methanothermus sociabilis*. Eur. J. Biochem. **199:**147–152.
9. **Fairbanks, G., T. L. Steck, and D. F. H. Wallach.** 1971. Electrophoretic analysis of the major polypeptides of the human erythrocyte membrane. Biochemistry **10:**2606–2617.
10. **Ferry, J. G., P. H. Smith, and R. S. Wolfe.** 1974. *Methanospirillum*, a new genus of methanogenic bacteria, and characterization of *Methanospirillum hungatii* sp. nov. Int. J. Syst. Bacteriol. **24:**465–469.
11. **Graham, L. L., and T. J. Beveridge.** 1986. Evaluation of freeze-substitution and conventional embedding protocols for routine electron microscopic processing of eubacteria. J. Bacteriol. **172:**2141–2149.
12. **Hegerl, R.** 1992. A brief survey of software packages for image processing in biological electron microscopy. Ultramicroscopy **46:**417–423.
13. **Hovmöller, S., A. Sjögren, and D. N. Wang.** 1988. The structure of crystalline bacterial surface layers. Prog. Biophys. Mol. Biol. **51:**131–163.
14. **Kist, M. L., and R. G. E. Murray.** 1984. Components of the regular surface array of *Aquaspirillum serpens* MW5 and their assembly in vitro. J. Bacteriol. **157:**599–606.
15. **König, H.** 1988. Archaeobacterial cell envelopes. Can. J. Microbiol. **34:**395–406.
16. **König, H., and K. O. Stetter.** 1986. Studies on archaebacterial S layers. Syst. Appl. Microbiol. **7:**300–309.
17. **Koval, S. F., and K. F. Jarrell.** 1987. Ultrastructure and biochemistry of the cell wall of *Methanococcus voltae*. J. Bacteriol. **169:**1298–1306.
18. **Laemmli, U. K.** 1970. Cleavage of structural proteins during the assembly of the head of bacteriophage T4. Nature (London) **127:**680–685.
19. **Lechner, J., and M. Sumper.** 1987. The primary structure of a procaryotic glycoprotein. Cloning and sequencing of the cell surface glycoprotein of halobacteria. J. Biol. Chem. **262:**9724–9729.
20. **Lembcke, G., R. Dürr, R. Hegerl, and W. Baumeister.** 1991. Image analysis and processing of an imperfect two-dimensional crystal: the surface layer of the archaebacterium *Sulfolobus acidocaldarius* re-investigated. J. Microsc. **161:**263–278.
21. **Mescher, M. F., and J. L. Strominger.** 1976. Purification and characterization of a procaryotic glycoprotein from cell envelope of *Halobacterium salinarium*. J. Biol. Chem. **251:**2005–2014.
22. **Messner, P., D. Pum, M. Sára, K. O. Stetter, and U. B. Sleytr.** 1986. Ultrastructure of the cell envelope of the archaebacteria *Thermoproteus tenax* and *Thermoproteus neutrophilus*. J. Bacteriol. **166:**1046–1054.
23. **Messner, P., and U. B. Sleytr.** 1992. Crystalline bacterial cell-surface layers. Adv. Microb. Physiol. **33:**213–275.
24. **Nußer, E., and H. König.** 1987. S layer studies on three species of *Methanococcus* living at different temperatures. Can. J. Microbiol. **33:**256–261.
25. **Pangborn, J., and M. P. Starr.** 1966. Ultrastructure of *Lampropedia hyalina*. J. Bacteriol. **91:**2025–2030.
26. **Patel, G. B., and L. A. Roth.** 1977. Effect of sodium chloride on growth and methane production of methanogens. Can. J. Microbiol. **23:**893–897.
27. **Patel, G. B., L. A. Roth, L. van den Berg, and D. S. Clark.** 1976. Characterization of a strain of *Methanospirillum hungatii*. Can. J. Microbiol. **22:**1404–1410.
28. **Patel, G. B., G. D. Sprott, R. W. Humphrey, and T. J. Beveridge.** 1986. Comparative analysis of the sheath structures of *Methanothrix concilii* GP6 and *Methanospirillum hungatei* strains GP1 and JF1. Can. J. Microbiol. **32:**623–631.
29. **Phipps, B. M., R. Huber, and W. Baumeister.** 1991. The cell envelope of the hyperthermophilic archaebacterium *Pyrobaculum organotrophum* consists of 2 regularly arrayed protein layers—3-dimensional structure of the outer layer. Mol. Microbiol. **5:**253–265.
30. **Sára, M., and U. B. Sleytr.** 1987. Molecular sieving through S layers of *Bacillus stearothermophilus* strains. J. Bacteriol. **169:**4092–4098.
31. **Saxton, W. O., and W. Baumeister.** 1982. The correlation averaging of a regularly arranged bacterial cell envelope protein. J. Microsc. **127:**127–138.
32. **Schultze-Lam, S., G. Harauz, and T. J. Beveridge.** 1992. Participation of a cyanobacterial S layer in fine-grain mineral formation. J. Bacteriol. **174:**7971–7981.

32a. **Southam, G.** Personal communication.

33. **Southam, G., and T. J. Beveridge.** 1991. Dissolution and immunochemical analysis of the sheath of the archaeobacterium *Methanospirillum hungatei* GP1. J. Bacteriol. **173:**6213–6222.
34. **Southam, G., and T. J. Beveridge.** 1992. Characterization of novel,

phenol-soluble polypeptides which confer rigidity to the sheath of *Methanospirillum hungatei* GP1. J. Bacteriol. **174:**935–946.
35. **Southam, G., and T. J. Beveridge.** 1992. Detection of growth sites in and protomer pools for the sheath of *Methanospirillum hungatei* GP1 by use of constituent organosulfur and immunogold labeling. J. Bacteriol. **174:**6460–6470.
36. **Southam, G., M. Firtel, B. L. Blackford, M. H. Jericho, W. Xu, P. J. Mulhern, and T. J. Beveridge.** 1993. Transmission electron microscopy, scanning tunneling microscopy, and atomic force microscopy of the cell envelope layers of the archaeobacterium *Methanospirillum hungatei* GP1. J. Bacteriol. **175:**1946–1955.
37. **Sprott, G. D., T. J. Beveridge, G. B. Patel, and G. Ferrante.** 1986. Sheath disassembly in *Methanospirillum hungatei* strain GP1. Can. J. Microbiol. **32:**847–854.
38. **Sprott, G. D., J. R. Colvin, and R. C. McKellar.** 1979. Spheroplasts of *Methanospirillum hungatei* formed upon treatment with dithiothreitol. Can. J. Microbiol. **25:**730–738.
39. **Sprott, G. D., and R. C. McKellar.** 1980. Composition and properties of the cell wall of *Methanospirillum hungatei*. Can. J. Microbiol. **26:**115–120.
40. **Sprott, G. D., K. M. Shaw, and K. F. Jarrell.** 1983. Isolation and chemical composition of the cytoplasmic membrane of the archaebacterium *Methanospirillum hungatei*. J. Biol. Chem. **258:**4026–4031.
41. **Stewart, M., T. J. Beveridge, and G. D. Sprott.** 1985. Crystalline order to high resolution in the sheath of *Methanospirillum hungatei*: a cross-beta structure. J. Mol. Biol. **183:**509–515.
42. **Takano, T., and R. E. Dickersen.** 1981. Conformation change of cytochrome c. J. Mol. Biol. **153:**79–94.
43. **Timasheff, S. N., and T. Arakawa.** 1989. Stabilization of protein structure by solvents, p. 331–345. *In* T. E. Creighton (ed.), Protein structure: a practical approach. IRL Press, Oxford.
44. **Tsuboi, A., N. Tsukagoshi, and S. Udaka.** 1982. Reassembly in vitro of hexagonal surface arrays in a protein-producing bacterium, *Bacillus brevis* 47. J. Bacteriol. **151:**1485–1497.
45. **Wildhaber, I., U. Santarius, and W. Baumeister.** 1987. Three-dimensional structure of the surface protein of *Desulfurococcus mobilis*. J. Bacteriol. **169:**5563–5568.
46. **Woese, C. R., and G. J. Olsen.** 1986. Archaebacterial phylogeny: perspectives on the urkingdoms. Syst. Appl. Microbiol. **7:**161–177.